JCTC Journal of Chemical Theory and Computation

Article

pubs.acs.org/JCTC

Spins Dynamics in a Dissipative Environment: Hierarchal Equations of Motion Approach Using a Graphics Processing Unit (GPU)

Masashi Tsuchimoto and Yoshitaka Tanimura*

Department of Chemistry, Graduate School of Science, Kyoto University, Sakyoku, Kyoto 606-8502, Japan

Supporting Information

ABSTRACT: A system with many energy states coupled to a harmonic oscillator bath is considered. To study quantum non-Markovian system-bath dynamics numerically rigorously and nonperturbatively, we developed a computer code for the reduced hierarchy equations of motion (HEOM) for a graphics processor unit (GPU) that can treat the system as large as 4096 energy states. The code employs a Padé spectrum decomposition (PSD) for a construction of HEOM and the exponential integrators. Dynamics of a quantum spin glass system are studied by calculating the free induction decay signal for the cases of 3×2 to 3×4 triangular lattices with antiferromagnetic interactions. We found that spins relax faster at lower temperature due to transitions through a quantum coherent state, as represented by the off-diagonal elements of the reduced density matrix, while it has been known that the spins relax slower due to suppression of thermal activation in a classical case. The decay of the spins are qualitatively similar regardless of the lattice sizes. The pathway of spin relaxation is analyzed under a sudden temperature drop condition. The Compute Unified Device Architecture (CUDA) based source code used in the present calculations is provided as Supporting Information.

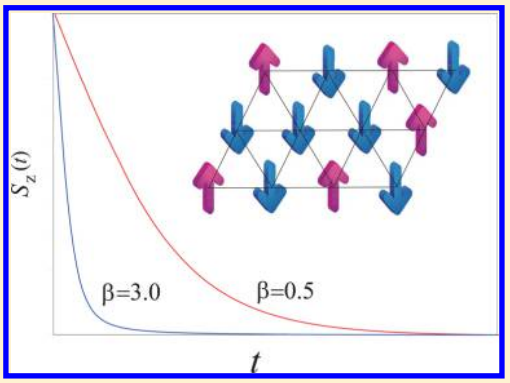

1. INTRODUCTION

Quantum open systems have been a subject of fundamental interest in physics, chemistry, and biology for many years.[1] Problems in this category include quantum information,[2] electron and exciton transfer,[3] and time-resolved nonlinear spectroscopy.[4] A widely used model for an quantum open system consists of a main system represented in terms of energy states or configuration states, which is in turn coupled to heat-bath consisting of an ensemble of harmonic oscillators.[1,2] While the model itself is fairly simple, it is difficult to study dynamics analytically and even numerically, due to the infinite number of bath degrees of freedom. A great deal of effort has been dedicated to numerically calculating the time evolution of this model system, and several numerically rigorous approaches have been developed for the spin-Boson system and Brownian oscillator system. These approaches involve the quasi-adiabatic propagator path integral (QUAPI),[5] the numerical renormalization group (NRG),[6] and the reduced hierarchy equations of motion (HEOM) approach.[7−25] Although the relaxation process of a model system under external perturbations is now well understood, that of complex system consisting of a spatially distributed multilevel subsystems and a potential system defined in a multidimensional configuration space have not been well explored due to a lack of computational power. To overcome the size limitation of the system, several computational efforts have been made. In this regard, the HEOM approach, which is defined by a simultaneous differential equations for the density matrix elements, are fitted in contemporary computer architecture that consists of many CPUs and large shared and distributed memories. The codes based on a Message passing interface (MPI),[20] Graphics processing unit (GPU),[21−24] and the Open computer language (OpenCL)[25] have been developed to study photosynthetic antenna systems. Several algorithms have also been introduced to reduce the size limitation.[14−19]

In the present paper, we developed a HEOM program for GPUs that is specifically designed to treat a quantum Ising system defined in many energy states. It should be noted that the scaling of the computational costs versus the system size is different for the photosynthesis case and for the quantum Ising case. In the photosynthesis case, we have to treat the fluctuation described by a complex bath spectral distribution that can be different in each site, while the system-bath coupling is not strong and the bath temperature is high. In the quantum Ising case, we describe the relaxation process by a single Drude heat bath, while the system-bath integration is not weak and the bath temperature can be very low. Nevertheless, the major limitation of both cases arises from the system size, because we have to treat the reduced density matrix instead of the wave function.

This paper is organized as follows. In Section 2, we present the model Hamiltonian and HEOM. In Section 3, we explain the optimized methodology for coding the HEOM to treat large system. We then show how this code can be used to calculate and analyze free induction decay signal of quantum

Received: May 25, 2015
Published: July 21, 2015

DOI: 10.1021/acs.jctc.5b00488
J. Chem. Theory Comput. 2015, 11, 3859−3865

spin glass in Section 4. Section 5 is devoted to concluding remarks.

2. REDUCED HIERACHAL EQUATIONS OF MOTION

We consider a quantum system coupled to a harmonic oscillator bath. The Hamiltonian is written as[1−3,10−12]

$$\hat{H}_{tot} = \hat{H}_A + \sum_j \left[\frac{\hat{p}_j^2}{2m_j} + \frac{m_j\omega_j^2}{2}\left(\hat{x}_j - \frac{\alpha_j \hat{V}}{m_j\omega_j^2}\right)^2 \right] \tag{1}$$

where m_j, $\hat{p}_j$, $\hat{x}_j$, and ω_j are the mass, momentum, position, and frequency variables of the jth oscillator mode, and $\hat{V}$ is the system part of the interaction, and α_j is the coupling constant between the system and the jth oscillator. The heat bath can be characterized by the spectral distribution function, $J(\omega) = \sum_j \alpha_j^2 \delta(\omega-\omega_j)/(2m_j\omega_j)$, and the inverse temperature, $\beta = 1/kT$, where k is the Boltzmann constant. We assume the Drude distribution, given by[7,8]

$$J(\omega) = \frac{\eta}{\pi}\frac{\gamma^2\omega}{\omega^2+\gamma^2} \tag{2}$$

where the constant γ represents the width of the spectral distribution of the collective phonon modes and is the reciprocal of the correlation time of the noise induced by the bath at the high temperature. The parameter η is related to the system-bath coupling strength. Because we are typically not interested in the bath degrees of freedom, we can consider a reduced density operator $\hat{\rho}_A = \mathrm{tr}_B\{\hat{\rho}_{tot}\}$, which is the partial trace of the total density operator over the bath degrees of freedom. We then employ the reduced hierarchy equations of motion (HEOM) approach, which can be used to treat non-Markovian and nonperturbative system-bath interactions at finite temperature in a numerically rigorous way.[7−13] In the HEOM formalism, the reduced density operator is expressed in terms of the auxiliary hierarchy density matrix elements, $\hat{\rho}^{(n)}_{j_1,\cdots,j_K}$, where the indices n and j_k arise from the hierarchal expansion of the decay functions $e^{-\gamma t}$ and $e^{-\nu_k t}$ with the kth Matsubara frequency, $\nu_k = 2\pi k/\beta\hbar$. Then the zeroth element is identical to $\hat{\rho}^{(0)}_{0,0,\cdots,0}(t) = \hat{\rho}_A(t)$.

Dynamics of the reduced density operator for the system described by eqs 1 and 2 are expressed in hierarchical form as[8−11]

$$\begin{aligned}\frac{\partial}{\partial t}\hat{\rho}^{(n)}_{j_1,\cdots,j_K}(t) = &-\left[i\hat{\mathcal{L}} + n\gamma + \sum_{k=1}^{K}(j_k\nu_k + \hat{\Phi}\hat{\Psi}_k) + \hat{\Xi}\right]\hat{\rho}^{(n)}_{j_1,\cdots,j_K}(t)\\ &- \hat{\Phi}\hat{\rho}^{(n+1)}_{j_1,\cdots,j_K}(t) - n\gamma\hat{\Theta}\hat{\rho}^{(n-1)}_{j_1,\cdots,j_K}(t)\\ &- \sum_{k=1}^{K}\hat{\Phi}\hat{\rho}^{(n)}_{j_1,\cdots,j_{k+1},\cdots,j_K}(t) - \sum_{k=1}^{K} j_k\nu_k\hat{\Psi}_k\hat{\rho}^{(n)}_{j_1,\cdots,j_{k-1},\cdots,j_K}(t)\end{aligned} \tag{3}$$

Here, $i\hat{\mathcal{L}}$ is the quantum Liouvillian of the system, and other operators are defined by $\hat{\Phi} \equiv i\hat{V}^{\times}/\hbar$, $\hat{\Psi}_k \equiv i\eta c_k\hat{V}^{\times}/\beta\hbar$

$$\hat{\Theta} \equiv \frac{i\eta}{\beta\hbar}\left[-i\frac{\beta\hbar\gamma}{2}\hat{V}^{\circ} + \frac{\beta\hbar\gamma}{2}\cot\left(\frac{\beta\hbar\gamma}{2}\right)\hat{V}^{\times}\right] \tag{4}$$

and

$$\hat{\Xi} \equiv \frac{\eta}{\beta\hbar^2}\left[1 - \frac{\beta\hbar\gamma}{2}\cot\left(\frac{\beta\hbar\gamma}{2}\right)\right]\hat{V}^{\times}\hat{V}^{\times} + i\frac{\eta}{\beta\hbar^2}\frac{\beta\hbar\gamma}{2}\hat{V}^{\circ}\hat{V}^{\times} \tag{5}$$

where $c_k = 2\gamma^2/(\nu_k^2-\gamma^2)$ and $\hat{V}^{\times}\hat{f} \equiv \hat{V}\hat{f} - \hat{f}\hat{V}$ and $\hat{V}^{\circ}\hat{f} \equiv \hat{V}\hat{f} + \hat{f}\hat{V}$ for any operator $\hat{f}$. When the combinations of n and j_k are sufficiently large that the condition $N \equiv n + \sum_{k=1}^{K} j_k \gg \omega_0/\min(\gamma,\nu_1)$ holds, the infinite hierarchy in eq 3 can be truncated at those values of n and j_k with negligible error by setting[9]

$$\frac{\partial}{\partial t}\hat{\rho}^{(n)}_{j_1,\cdots,j_K}(t) \simeq -\left(i\hat{\mathcal{L}} + \sum_{k=1}^{K}\hat{\Phi}\hat{\Psi}_k + \hat{\Xi}\right)\hat{\rho}^{(n)}_{j_1,\cdots,j_K}(t) \tag{6}$$

In principle, the HEOM provides an asymptotic approach that allows us to calculate various physical quantities with any desired accuracy by adjusting the number of hierarchal elements determined by N; the error introduced by the truncation is negligibly small when N is sufficiently large.

3. NUMERICAL INTEGRATION METHODS

3.1. Padé Spectrum Decomposition. In order to construct the HEOM, we expanded $\coth((\beta\hbar\omega)/2)$ in terms of Matsubara frequencies as

$$\coth\left(\frac{\beta\hbar\omega}{2}\right) \simeq \frac{2}{\beta\hbar\omega} + \frac{4}{\beta\hbar}\sum_j \frac{\omega}{\omega^2+\nu_j^2} \tag{7}$$

While the HEOM from above expression leads to the classical limit naturally for $\hbar \to 0$,[12] this expansion is not convenient for numerical calculations, because the number of hierarchy elements constructed from this expression becomes very large specifically at low temperature. Thus, in order to reduce the hierarchy size, the Padé spectrum decomposition (PSD) was developed.[14−17] Here, we adapt [N-1/N] PSD for the Bose distribution, which can be easily implemented in the HEOM code in the conventional expression. We thus expand $\coth((\beta\hbar\omega)/2)$ into

$$\coth\left(\frac{\beta\hbar\omega}{2}\right) \simeq \frac{2}{\beta\hbar\omega} + \frac{4}{\beta\hbar}\sum_j^{K} \frac{\omega\zeta_j}{\omega^2 + \left(\frac{\xi_j}{\beta\hbar}\right)^2} \tag{8}$$

where ζ_j are given by

$$\zeta_j = \frac{1}{2}K(2K+3)\prod_{k=1}^{K-1}(\zeta_k^2 - \xi_j^2)/\prod_{k=1,k\neq j}^{K}(\xi_k^2 - \xi_j^2) \tag{9}$$

where the parameters $\zeta_j \equiv 1/\tilde{\lambda}_j$ and $\xi_j \equiv 1/\lambda_j$ are determined from the sorted eigenvalues of the matrix λ_j and $\tilde{\lambda}_j$, whose elements are expressed as

$$\Lambda_{mn} = \frac{\delta_{m,n\pm1}}{\sqrt{(2m+1)(2n+1)}} \tag{10}$$

for $m, n = 1, 2, \ldots, 2K$ and

$$\tilde{\Lambda}_{mn} = \frac{\delta_{m,n\pm1}}{\sqrt{(2m+3)(2n+3)}} \tag{11}$$

for $m, n = 1, 2, \ldots, 2K-1$, respectively. Then, by simply replacing the Matsubara frequencies as $\nu_j = \xi_j/\beta\hbar$ and the coefficients c_k in $\hat{\Psi}_k$ as $c_k = 2\zeta_k\gamma^2/(\nu_k^2-\gamma^2)$, we can obtain the HEOM under PSD from eqs 3−6. The accuracy of PSD for different HEOM depth has been tested extensively for a spin-Boson system.[14−17] We found that the convergence of the HEOM in the present case follows the spin-Boson case.

DOI: 10.1021/acs.jctc.5b00488
J. Chem. Theory Comput. 2015, 11, 3859−3865

Chart 1. Calculations of the Liouvillian for $\hat{H}^{\times}\hat{\rho}^{(n)}_{j_1,\ldots,j_K}$ and $\hat{V}^{\times}\hat{\rho}^{(n)}_{j_1,\ldots,j_K}$ with the Use of cublasGemm in cuBLAS Library

```
//For double precisions, cublasC... -> cublasZ.., cuComplex ->
cuDoubleComplex __global__ void getdRhoKernel1( const cuComplex*
__restrict__ Rho, cuComplex* __restrict__ dRho, const cuComplex*
__restrict__ h, const cuComplex* __restrict__ v, cuComplex* buffer,
const int n) { cublasHandle_t handle;
  cublasError(cublasCreate(&handle)); int index=blockIdx.x;

        //Liouvillian
#ifdef H_DIAGONAL //if H is diagonal, treat H as a vector
        cublasCdgmm(handle,CUBLAS_SIDE_LEFT,n,n,Rho+index*n*n,n,h,n+1,
                                    dRho+index*n*n,n);
        cublasCgemm(handle,CUBLAS_OP_N,CUBLAS_OP_N,n,n,n,&minusiCnt,
                                    Rho+index*n*n,n,h,n,&iCnt,dRho+index*n*n,n);
#else
        Commutate(handle,h,Rho+index*n*n,&minusiCnt,n,dRho+index*n*n);
#endif
        Commutate(handle,v,Rho+index*n*n,&one,n,buffer+index*n*n);
        cublasDestroy(handle);
}

__device__ void Commutate(const cublasHandle_t &handle,
                                    const cuComplex* matrix1,const cuComplex* matrix2,
                                    const cuComplex* k,const int n,cuComplex* result)
{
        cublasStatus_t st1=cublasCgemm(handle,CUBLAS_OP_N,
                        CUBLAS_OP_N,n,n,n,k,matrix1,n,matrix2,n,&zero,result,n);
        cublasStatus_t st2=cublasCgemm(handle,CUBLAS_OP_N,
                        CUBLAS_OP_N,n,n,n,k,matrix2,n,matrix1,n,&minusOne,result,n);
        if(st1!=0||st2!=0){printf("%s","error\n");}
}
```

3.2. Exponential Integrator Method. The HEOM have been solved by numerically integrating in time using the Runge−Kutta method (RK4), which requires four times more memory than the memory stored in the HEOM elements. To reduce the memory size limitation of HEOM, Wilkins and Dattani[19] introduced the exponential integrator method developed by Al-Mohy and Higham.[26] Here, we outline this approach.

We consider the case that the hierarchal elements are expressed as the $M \times M$ density matrix with the elements $\hat{\rho}^{(n)}_{j_1,\ldots,j_K}(t)_{jk}$, where $1 \le j, k \le M$. The HEOM are the simultaneous differential equations in time that expressed in terms of ADOs in the matrix forma as

$$\frac{\partial \boldsymbol{\rho}}{\partial t} = \mathbf{X}\boldsymbol{\rho}(t) \tag{12}$$

where $\rho(t)$ is the vector determined by

$$\boldsymbol{\rho}(t) = \{\hat{\rho}^{(0)}_{0\ldots0}(t)_{11}, \hat{\rho}^{(0)}_{0\ldots0}(t)_{12}, \ldots, \hat{\rho}^{(0)}_{0\ldots0}(t)_{MM}, \hat{\rho}^{(1)}_{0\ldots0}(t)_{11}, \ldots\} \tag{13}$$

which contains all elements of each ADOs and $\mathbf{X}$ is the matrix that is constructed from the operators appear in eq 3. The formal solution of eq 12 is expressed in terms of Taylor series as

$$\begin{aligned}\boldsymbol{\rho}(t + \Delta t) &= \exp(\Delta t\mathbf{X})\boldsymbol{\rho}(t)\\ &= \boldsymbol{\rho}(t) + \sum_{j=1}^{\infty}\dot{\boldsymbol{\rho}}_j\end{aligned} \tag{14}$$

where

$$\dot{\boldsymbol{\rho}}_j \equiv \frac{(\Delta t\mathbf{X})^j\boldsymbol{\rho}(t)}{j!} \tag{15}$$

The vector elements, $\dot{\boldsymbol{\rho}}_j$, are determined from the recursive relations $\dot{\boldsymbol{\rho}}_0 \equiv \dot{\boldsymbol{\rho}}(t)$ and

$$\dot{\boldsymbol{\rho}}_j \equiv \frac{\Delta t\mathbf{X}}{j}\dot{\boldsymbol{\rho}}_{j-1} \tag{16}$$

for $j > 0$. We can calculate $\dot{\boldsymbol{\rho}}_j$ from $\dot{\boldsymbol{\rho}}_{j-1}$ by multiplying $\Delta t\mathbf{X}/j$. Because $\dot{\boldsymbol{\rho}}_{j-1}$ can be disregarded after evaluating $\dot{\boldsymbol{\rho}}_j$, we compute the integral with using only twice the memory size of the HEOM elements.

3.3. Graphics Processor Unit (GPU) Calculation. It was shown that a GPU, which utilizes fast access memory and super parallel architecture on board, is a powerful device to integrate the HEOM for a system with many degrees of freedom.[21−25] To take advantage of the super parallel architecture of GPU, we must avoid unnecessary memory transfer between the host computer and GPU device, because the memory access speed of the host is much slower than GPU memory. By adapting the Padé decomposition and exponential integrators, we can assign the required memory for numerical integrations on the GPU board for a system up to 4096 energy sites. We developed the GPU code for HEOM based on Compute Unified Device Architecture (CUDA), which is an extension of the C and C++ programming language for GPU developed by NVIDIA. In CUDA, a program which runs on the GPU device is called a kernel. Here, we present the kernels for Liouvillian defined by eqs 3−5 involved in the subroutine, Liouville.cu, to illustrate the operation. The computationally expensive part of solving the HEOM is the matrices multiplications of $\hat{H}$, $\hat{V}$, and $\boldsymbol{\rho}$ involved in the Liouvillian. To accelerate these calculations we employ a basic linear algebra library, cuBLAS, which is design for GPU kernel with dynamic parallelization reducing overhead costs of GPU calculations.

In our routine, the ADO density matrices $\boldsymbol{\rho}$ and $\dot{\boldsymbol{\rho}}$ are stored as the vector Rho and dRho, whose elements are specified by

DOI: 10.1021/acs.jctc.5b00488
J. Chem. Theory Comput. 2015, 11, 3859−3865

Chart 2. Calculations of Liouvillian for $\dot{\rho}$ Using the Elements Obtained in Chart 1

```
__global__ void getdRhoKernel2(
        const int* numbers, const int* edges,
        const cuComplex* __restrict__ Rho, cuComplex* __restrict__ dRho,
        const cuComplex* __restrict__ h, const cuComplex* __restrict__ v,
        const cuComplex* __restrict__ nu,
        const cuComplex kThetaCommutate, const cuComplex kThetaAntiCommutate,
        const cuComplex kXi, const cuComplex kXiCounter,
        const cuComplex* phi, cuComplex* buffer,
        const int kMax, const int jMax, const int n, const int size, cuComplex* tmp)
{
        cublasHandle_t handle;
        cublasError(cublasCreate(&handle));
        int index=blockIdx.x;
        //Phi
        for(int i=0;i<kMax+1;i++)
        {
        // edges[i] returns the index of ADO for i.
        // If edges[i] is larger than the index of terminator,
    // returns "buffer+size*n*n."
                int indexkPlus1=edges[index*(kMax*2+2)+i];
        // For termination, dRho for buffer+size*n*n is set to be zero.
                addMatrix(handle,n,&minusiCnt,dRho+index*n*n,
                                                buffer+indexkPlus1*n*n);
        }
        .
        .
        cublasDestroy(handle);
}
```

"index" of the $n \times n$ matrix, where $n = N \times M$. In order to evaluate the Liouvillian, we employ the cublasCdgmm function in cuBLAS to $\hat{H}_A^{\times}\hat{\rho}^{(n)}_{j_1,\ldots,j_K}$ and $\hat{V}^{\times}\hat{\rho}^{(n)}_{j_1,\ldots,j_K}$, while the left of the calculations adding results. To synchronize the results from cuBLAS to calculate dRho, we separate the routine for Liouvillian into two parts, as illustrated in Charts 1 and 2. Here, "__device__ " and "__global__ " are the function type qualifiers provided by CUDA to specify execution on the GPU and the host computer, respectively. The calculations are carried out within single precision, but we can change the precision by overwriting the definition of complex numbers, as instructed in Charts 1 and 2. The source code is provided as Supporting Information.

4. DYNAMICS OF QUANTUM SPIN GLASS SYSTEM

A spin glass is a complex system characterized by frustrated interactions that exhibits an irreversible dynamics of spins to metastable states without long-range spatial order below the glass transition temperature.[27] Contrastingly, quantum spin glass systems that have been identified in a number of materials[28] exhibit faster relaxation than a classical case due to the quantum transitions from metastable states to the ground state. This cooling mechanism, often referred to as quantum annealing, is employed to realize a quantum computation.[31−33] While the quantum annealing has been studied by applying a time-dependent transversal field, here we consider the case of a spin system that interacts with a harmonic heat-bath, which relaxes the system to the thermal equilibrium state of the total system at finite temperature. We consider a two-dimensional triangular spin−lattice system in a longitudinal magnetic field, expressed as[29,30]

$$\hat{H}_A = \sum_{i=1}^{L}\sum_{j=i+1}^{L} J_{ij}\sigma_i^z\sigma_j^z + \Gamma\sum_{i=1}^{L}\sigma_i^z \tag{17}$$

where σ_i are the Pauli matrices for the ith spin, Γ is the longitudinal magnetic field, and J_{ij} represents the strength of antiferromagnetic interaction between the nearest neighbor spins for the total number of the spin, L. In a quantum system-bath model, the thermal equilibrium state of the system is not a pure state of the system, $\exp(-\beta\hat{H}_A)$, but the reduced state of the total system, $\mathrm{tr}_B\{\exp[-\beta(\hat{H}_A + \hat{H}_I + \hat{H}_B)]\}$. Dynamical aspects of the bath are characterized by the fluctuation and dissipation upon the system dynamics, which are related through the quantum version of the fluctuation−dissipation theorem. Quantum noise is by nature non-Markovian, and the Matsubara frequencies, $\nu_k = 2\pi k/\beta\hbar$, play an essential role, in addition to quantum coherence between the system and environment.[10−13] To treat the entire system quantum mechanically in a consistent and rigorous fashion, we have to expand the scope of the Hamiltonian, eq 17, by including the coupling to the surrounding environment represented by eq 1 with eq 2. Here, we chose the system part of system-bath interaction

$$\hat{V} = \sum_{i=1}^{L}\left(\sigma_i^x + \frac{1}{2}\sigma_i^z\right) \tag{18}$$

which indicates that all spins interact with the single bath system. Then, for spectral distribution, eq 2, non-Markovian and nonperturbative dynamics of the reduced system can be studied by integrating the HEOM, eqs 3−6.

Because the number of states involved in the L spins system is 2^L, it is not easy to study a large system. Using the methodology explained in the previous section, we treat the spin system with up to 12 spins, which involves 4096 energy states. Note that we do not use periodic boundary conditions, because our system is so small that this condition is unrealistic and, because it may be possible to find a small system similar to a present model experimentally, in a microscopic material. We set $\Gamma = 1/2$ and $J_{ij} = 0.15$ and the system-bath parameters as $\eta = 0.01$ and $\gamma = 1$. We carried out numerical calculation using

DOI: 10.1021/acs.jctc.5b00488
J. Chem. Theory Comput. 2015, 11, 3859−3865

NVIDIA Tesla K20 and K80 with CUDA toolkit 6.5. We chose the depth of the hierarchy and the number of ADOs in PSD representation as $N = 3$ and $K = 2$, as a result the total numbers of the hierarchy elements used in calculations are $N_{tot} = 10$. The computing time of both cuSPARSE and cuBLAS programs on Tesla K20 are 160 ms per step for time evolution of 9 spins system. We found that the program with cuSPARSE is faster than that with cuBLAS when the number of spins is more than 7. For 12 spins system run on NVIDIA Tesla K80, the computing time of program is 4.5 s/step with cuSPARSE on Tesla K80.

4.1. Free Induction Decay. We calculate the free induction decay signal defined by the spin expectation value $\langle S_z(t)\rangle$ with the initial configuration where all spins are upward, i.e. $\langle S_z(0)\rangle = 1$, where $\langle S_z(t)\rangle = \sum_j^L \langle \hat{\sigma}_j^z \hat{\rho}_A(t)\rangle / L$. If the external field is zero, the situation corresponds to zero field NMR or μSR measurements.[9] The simulation begins from this situation, in which all spins are upward for the bath temperature $\beta\hbar = 0.5$ and 3. Figure 1 illustrates the relaxation of $S_z(t) \equiv (\langle S_z(t)\rangle - \langle S_z(\infty)\rangle)/(\langle S_z(0)\rangle - \langle S_z(\infty)\rangle)$. In a classical case, spins relax faster for higher temperature.[27] In a quantum case, however, we found that spins relax faster for lower temperature due to the transitions through the quantum coherent state, represented by the off-diagonal elements of the reduced density matrix. The decays of spins are similar regardless of the lattice sizes. Like a spin-Boson system,[9] which corresponds to the 1×1 case in the present model, the FID signal decays as neither exponential nor a stretch exponential form. This is because the relaxation in the present case is characterized by the transitions between the energy eigenstates through the nonperturbative system-bath interactions at finite temperature. Due to the non-Markovian nature of the dissipation and fluctuation, the system relaxes to the thermal equilibrium state nonexponentially,[10,13] while the local energy minimum states play a minor role in the quantum case due to the coherent transitions. Although we could increase the lattice size only up to 3×4, the spins decays in a similar manner regardless of the size. This is because, while the bath coupled to all of the spins strongly, the spin−spin interactions are weak and localized. We should note that the profile of $S_z(t)$ is similar to the profile of the system energy

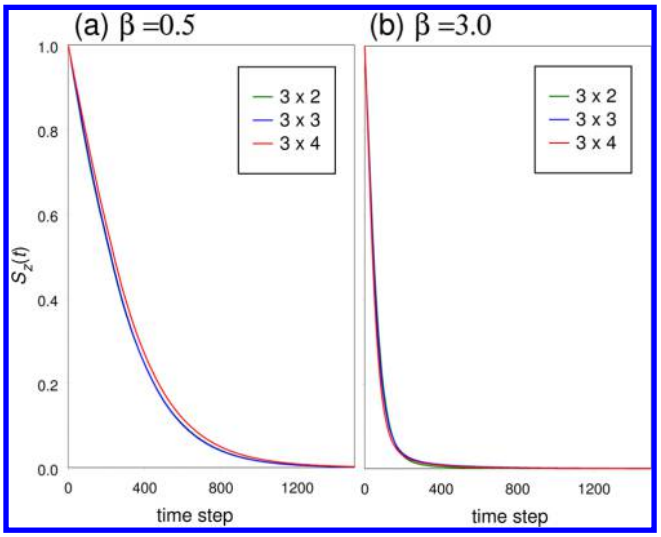

Figure 1. Free induction decay signal of spin, $S_z(t)$, in 3×2, 3×3, and 3×4 triangular spin−lattice for (a) the high temperature case, $\beta = 0.5$, and (b) the low temperature case, $\beta = 3.0$.

$\mathrm{tr}\{\hat{H}_A \rho_{tot}(t)\}$, because the contribution of energy from the spin−spin interactions is smaller than that from the system-bath coupling.

4.2. Linear Response to Temperature Jump. We next study the response of the system to a sudden temperature drop of the heat-bath. For a small temperature jump, the observable of this measurement corresponds to magnetic susceptibility. Focusing on 3×3 triangular lattice, we first equilibrate the system at $\beta\hbar = 1$ by running the program for a sufficiently long time ($t = 10000$). Then we drop the bath temperature to $\beta\hbar = 10$ suddenly to observe the spin relaxation toward the new equilibrium state in time. Figure 2 depicts the relaxation of the

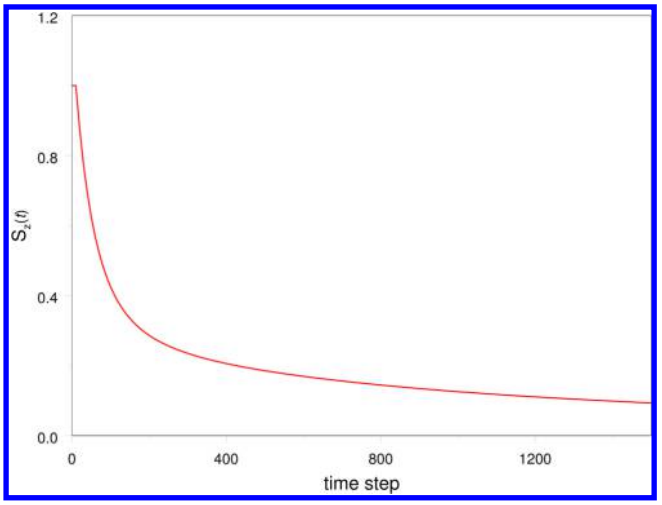

Figure 2. Time evolution of $S_z(t)$ after the sudden temperature drop is plotted for 3×3 triangular lattice.

spin expectation value after the temperature change. Because the thermal equilibrium state of the total system is a mixed state (or unfactorized state) of the system and the bath in the quantum case, there exist the initial system-bath coherence in the present case, whereas we ignored this effect in the FID case. Thus, the signal from the temperature jump exhibits a slight delay of response ($t < 10$), while the FID signal decays monotonically. We found that the decay profile of the signal in Figure 2 is similar to the 3×3 case of the signal in Figure 1 for $t > 100$ indicating that, other than the initial correlation, the decay process in the temperature drop is similar to the FID case. If we wish to study system-bath coherence further, it is more instructive to study nonlinear response functions, as demonstrated in the spin-Boson and Brownian oscillator cases.[10−13]

Here, we also analyze the relaxation pathways using the density matrix elements as a function of times. Figure 3 illustrates the representative relaxation pathway from a local minimum state to the ground state with their spin configuration. Initially, the population of the local minimum state (i) increases because the energy from other states (involving (a) and (b)) flow into (i) after the temperature change. The population of (i) transfers to (ii), while the transition between (i) and (iii) are negligible. This can be monitored from the change of the off-diagonal elements of the density matrix between (i) and (ii) and between (i) and (iii). The population in (ii) then finally relaxes to the ground state (iii) with losing energy due to the bath. We should note that the transition between (i) and (ii) does not occur through a classical single-spin-flip transition.[34] Possible pathways from (i)

DOI: 10.1021/acs.jctc.5b00488
J. Chem. Theory Comput. 2015, 11, 3859−3865

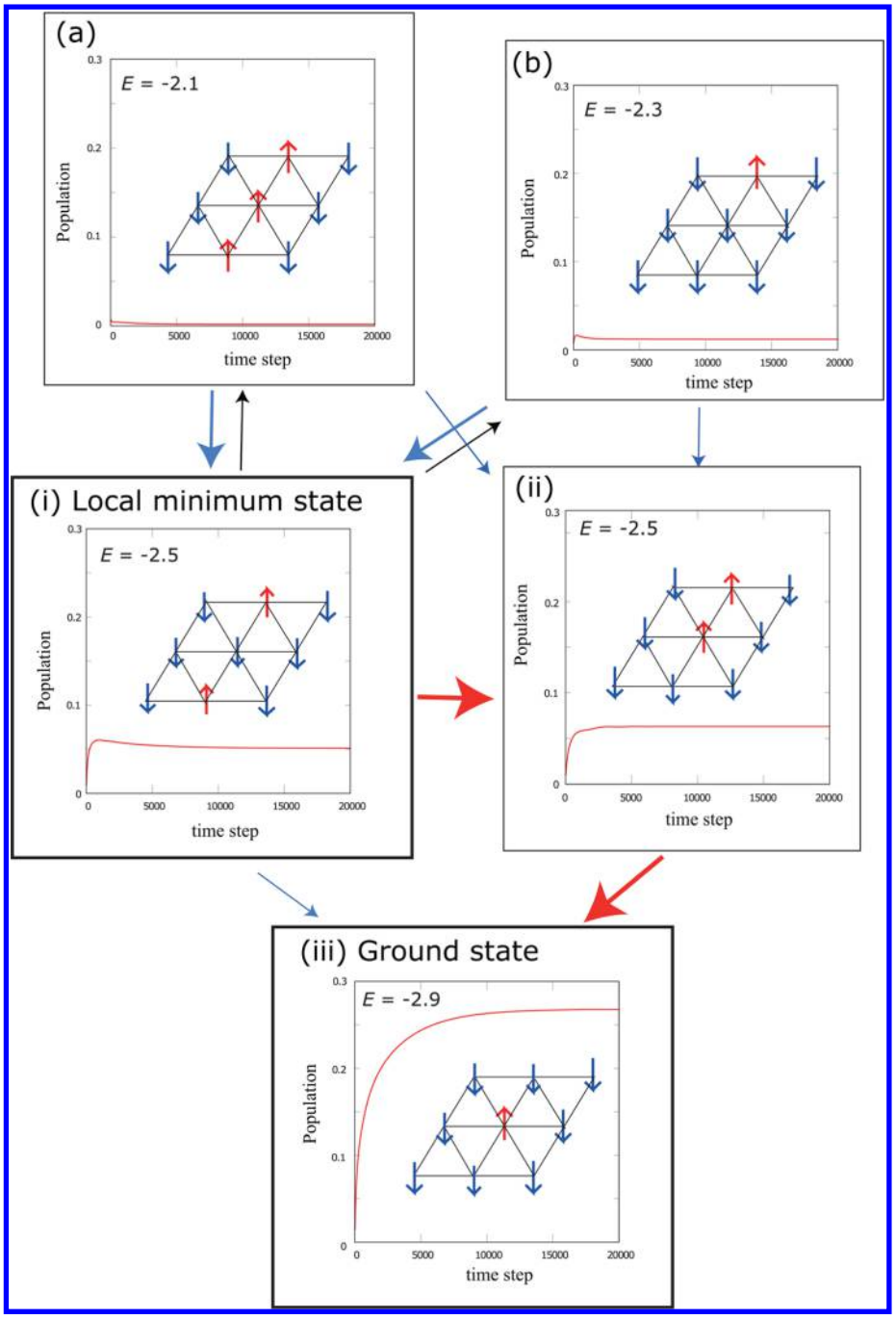

Figure 3. A possible energy transfer paths from (i) a local minimum state to (iii) the grand minimum state through the transition state (ii) illustrated with their spin configurations. The red arrows indicate the dominant quantum transition, while black arrows indicate classical paths via single-spin-flip processes.

to (ii) in classical mechanics are through (a) or (b), as indicated in the blue arrows in Figure 3. Although (i) is a local minimum state in classical mechanics, it is not in the quantum case, as indicated by the smooth transition between (i) and (ii). This is a key feature of quantum annealing that has been used to develop quantum computer.[31,32]

5. CONCLUSION

Using a GPU-based computer program for HEOM, we studied non-Markovian and nonperturbative quantum dissipative dynamics for triangular antiferromagnetic spin-glass systems of sizes up to 3 × 4, which involves 4096 energy states, in a numerically rigorous fashion. A compressed exponential decay of FID signals was observed. The size dependence of the decay profiles were found to be minor, even when we considered the open boundary condition. Relaxation pathways were studied using the calculated density matrix elements under temperature jump measurements. The microscopic picture of quantum annealing professes were illustrated. This result also indicates the capability of simulating quantum computing process in a rigorous quantum mechanically fashion.

Although here we treated spin systems only, the present methodology can handle any system described by energy eigenstates. The extension to a Brownian[35−37] and a more

DOI: 10.1021/acs.jctc.5b00488
J. Chem. Theory Comput. 2015, 11, 3859−3865

general spectral distribution[24,25] should also be possible. Thus, the present code can be applied to exciton and electron transfer problems and vibrational and electronic spectroscopies that are described by the energy states.

In order to make the present approach more useful, further computational efforts have to be made to treat larger systems consisting of hundreds of spins. By using OpenCL code and distributing the computations over hundreds of CPU and GPU nodes, we may treat this kind of system.[25] Once we treat a reasonably large spin system, it is possible to compare the relaxation process of spins for the system-bath model and that for a large isolated system.[38] This direction of study allows us to explore the difference between the dynamics under the canonical and microcanonical ensembles under quantum mechanical situations.

■ ASSOCIATED CONTENT

Supporting Information

The source code of GPU-HEOM for a quantum Ising system. The Supporting Information is available free of charge on the ACS Publications website at DOI: 10.1021/acs.jctc.5b00488.

■ AUTHOR INFORMATION

Corresponding Author

*Phone: 81-75-753-4017. E-mail: tanimura@kuchem.kyoto-u.ac.jp.

Notes

The authors declare no competing financial interest.

■ ACKNOWLEDGMENTS

The authors are grateful for useful comments on the exponential integrator for the HEOM with Dr. Nikesh Dattani. The authors would like to thank HPC Systems Inc. for providing Tesla K80 machine, HPC5000-XHGPU4TS, to test our GPU code. The financial support from a Grant-in-Aid for Scientific Research (A26248005) from the Japan Society for the Promotion of Science is acknowledged.

■ REFERENCES

(1) Weiss, U. *Quantum Dissipative Systems*, 4th ed.; World Scientific: Singapore, 2012.
(2) Breuer, H. P.; Petruccione, F. *The Theory of Open Quantum Systems*; Oxford University Press: New York, 2002.
(3) Schröter, M.; Ivanov, S. D.; Schulze, J.; Polyutov, S. P.; Yan, Y.-J.; Pullerits, T.; Kühn, O. *Phys. Rep.* **2015**, *567*, 1(2015).
(4) Mukamel, S. *Principles of Nonlinear Optical Spectroscopy*; Oxford University Press: New York, 1995.
(5) Makri, N. *J. Chem. Phys.* **2014**, *141*, 134117.
(6) Chin, A. W.; Rivas, A.; Huelga, S. F.; Plenio, M. B. *J. Math. Phys.* **2010**, *51*, 092109.
(7) Tanimura, Y.; Kubo, R. *J. Phys. Soc. Jpn.* **1989**, *58*, 101−114.
(8) Tanimura, Y. *Phys. Rev. A: At., Mol., Opt. Phys.* **1990**, *41*, 6676.
(9) Ishizaki, A.; Tanimura, Y. *J. Phys. Soc. Jpn.* **2005**, *74* (12), 3131−3134.
(10) Tanimura, Y. *J. Phys. Soc. Jpn.* **2006**, *75*, 082001.
(11) Tanimura, Y. *J. Chem. Phys.* **2014**, *141*, 044114.
(12) Tanimura, Y. *J. Chem. Phys.* **2015**, *142*, 144110.
(13) Dijkstra, A. G.; Tanimura, Y. *Phys. Rev. Lett.* **2010**, *104*, 250401.
(14) Shi, Q.; Chen, L. P.; Nan, G. J.; Xu, R.-X.; Yan, Y.-J. *J. Chem. Phys.* **2009**, *130*, 084105.
(15) Hu, J.; Xu, R.-X.; Yan, Y.-J. *J. Chem. Phys.* **2010**, *133*, 101106.
(16) Hu, J.; Luo, M.; Jiang, F.; Xu, R.-X.; Yan, Y.-J. *J. Chem. Phys.* **2011**, *134*, 244106.
(17) Ding, J. J.; Xu, X.; Hu, J.; Xu, R.-X.; Yan, Y.-J. *J. Chem. Phys.* **2011**, *135*, 164107.
(18) Hou, D.; Wang, S.; Wang, R.; Ye, L.; Xu, R.-X.; Yan, Y.-J. *J. Chem. Phys.* **2015**, *142*, 104112.
(19) Wilkins, D. M.; Dattani, N. S. *J. Chem. Theory Comput.* **2015**, *11*, 3411.
(20) Strümpfer, J.; Schulten, K. *J. Chem. Theory Comput.* **2012**, *8*, 2808−2816.
(21) Kreisbeck, C.; Kramer, T.; Rodríguez, M.; Hein, B. *J. Chem. Theory Comput.* **2011**, *7*, 2166−2179.
(22) Kreisbeck, C.; Kramer, T. *J. Phys. Chem. Lett.* **2012**, *3*, 2828.
(23) Hein, B.; Kreisbeck, C.; Kramer, T.; Rodríguez, M. *New J. Phys.* **2012**, *14*, 023018.
(24) Kreisbeck, C.; Kramer, T.; Aspuru-Guzik, A. *J. Phys. Chem. B* **2013**, *117*, 9380.
(25) Kreisbeck, C.; Kramer, T.; Aspuru-Guzik, A. *J. Chem. Theory Comput.* **2014**, *10*, 4045−4054.
(26) Al-Mohy, A. H.; Higham, N. J. *SIAM. J. Sci. Comput.* **2011**, *33* (2), 488−511.
(27) Fischer, K. H.; Hertz, J. A. *Spin Glasses*; Cambridge University Press: 1991.
(28) Bitko, R.; Rosenbaum, T. F.; Aeppli, G. *Phys. Rev. Lett.* **1996**, *77*, 940−943.
(29) Wu, W.; Ellman, B.; Rosenbaum, T. F.; Aeppli, G.; Reich, D. H. *Phys. Rev. Lett.* **1991**, *67*, 2076−2079.
(30) Banerjee, V.; Dattagupta, S. *Phys. Rev. B: Condens. Matter Mater. Phys.* **2003**, *68*, 054202.
(31) Kadowaki, T.; Nishimori, H. *Phys. Rev. E: Stat. Phys., Plasmas, Fluids, Relat. Interdiscip. Top.* **1998**, *58*, 5355−5363.
(32) Suzuki, S.; Inoue, J.; Chakrabarti, B. K. *Quantum Ising Phases and Transitions in Transverse Ising Models*; Lecture Notes in Physics, Springer.
(33) Heim, B.; Ronnow, T. F.; Isakov, S. V.; Troyer, M. *Science* **2015**, *348*, 215−217.
(34) Glauber, R. J. *J. Math. Phys.* **1963**, *4*, 294−307.
(35) Tanaka, M.; Tanimura, Y. *J. Phys. Soc. Jpn.* **2009**, *78*, 073802.
(36) Tanaka, M.; Tanimura, Y. *J. Chem. Phys.* **2010**, *132*, 214502.
(37) Tanimura, Y. *J. Chem. Phys.* **2012**, *137*, 22A550.
(38) Niemeyer, H.; Michielsen, K.; De Raedt, H.; Gemmer, J. *Phys. Rev. E* **2014**, *89*, 012131.

DOI: 10.1021/acs.jctc.5b00488
J. Chem. Theory Comput. 2015, 11, 3859−3865